# MECHANO-FLUIDIC CHARACTERIZATION OF MICROSCALE DIELECTRIC BARRIER DISCHARGE PLASMA ACTUATORS

*J. C. Zito[1*], R. J. Durscher[2], J. Soni[2], S. Roy[2] and D. P. Arnold[1]*
[1]Interdisciplinary Microsystems Group, University of Florida, Gainesville, Florida, USA
[2]Applied Physics Research Group, University of Florida, Gainesville, Florida, USA

## ABSTRACT

This article reports the fluidic and mechanical thrust characterization of microscale dielectric barrier discharge plasma actuators intended for distributed flow control applications. Particle image velocimetry and pitot measurements indicate wall jet velocities up to 2.0 m/s while consuming an average power of 15 W/m of electrode. Direct force measurements using a torsional balance indicate a thrust up to 3 mN/m of electrode. These microscale actuators exhibit flow characteristics similar to macroscale DBD actuators, but with an order of magnitude reduction in footprint area and mass. Furthermore, compared to similar macroscale actuators, the "thrust effectiveness" (force divided by power) is similar, and the "velocity effectiveness" (velocity divided by power) is nearly doubled.

## INTRODUCTION

### Background & Motivation

Dielectric barrier discharge (DBD) plasma devices have received significant attention over recent years for applications such as active flow control, aero propulsion, biological sterilization, ozone generation, and microfluidic pumping. For active flow control applications, DBD devices offer the advantages of lack of moving parts, surface compliance, fast response and ease of construction, but generally suffer from low flow control authority (i.e. induced flow velocity, momentum transfer, and thrust).

Conventional DBD devices consist of two offset electrodes on either side of a dielectric material, as illustrated in Fig. 1. With high-voltage pulsed or AC excitation, the gas locally above the dielectric becomes weakly ionized creating a plasma discharge. This plasma imparts an electrohydrodynamic (EHD) force on the surrounding fluid, inducing a wall jet along the dielectric surface. Typical DBD actuators produce a wall jet with a velocity of 1 – 4 m/s occurring 0.5 – 1 mm above the dielectric surface. The net thrust produced ranges from a few mN/m to over 150 mN/m (thrust per unit length electrode), and the power consumption can range up to ~650 W/m, depending on both input voltage and frequency and the actuator geometry [1]. The actuator's "effectiveness"—output per consumed power—is a useful metric for comparing different designs operated at different voltage levels and frequencies. We apply this metric to define both "velocity effectiveness" (velocity divided by power) and "thrust effectiveness" (force divided by power) to compare the performance of DBD plasma actuators.

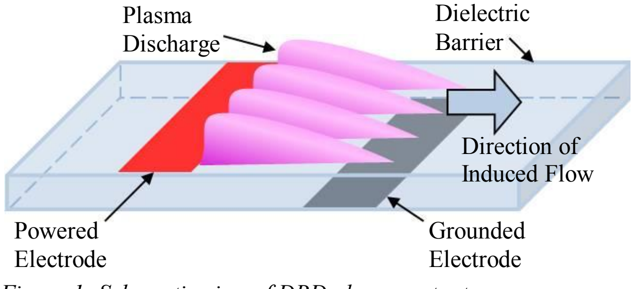


*Figure 1: Schematic view of DBD plasma actuator.*

For flow control applications, many efforts have been made to increase the control authority and/or effectiveness of DBD actuators by varying the input voltage amplitude and frequency, waveform shape (sinusoidal, pulsed, saw tooth, triangular, etc.), material properties, and device geometry. Extensive reviews of plasma actuators for use in flow control [2,3] summarize several trends that have been validated repeatedly in experiments. For example, the electrical power consumed scales exponentially with the sinusoidal input voltage amplitude [4], $P \propto V^{\alpha}$ with $\alpha \approx 3.5$. The thrust follows a similar scaling trend with voltage up to a certain saturation point, above which increasing the input no longer increases the force. Similarly, the induced velocity also saturates; maximum velocities of ~8 m/s have been experimentally demonstrated in standard atmospheric conditions [5].

The presence of the plasma imparts a Lorentzian force density ($F$) on the surrounding neutral fluid, which is a product of the applied electric field ($E$) and the net separated space charge density ($q$), $F = qE$. The fluidic control authority of the actuator is dependent on this force density and may be improved by increasing either the applied field or the space charge density. Increasing the electric field may be accomplished by simply increasing the voltage, reducing the dielectric thickness, or through geometric manipulation of the exposed electrode. For example, it has been shown that reducing the dielectric layer thickness increases the electric field resulting in an increase in measured thrust [1] (for a given input voltage/frequency). However, reducing the dielectric thickness may lead to dielectric breakdown and device failure. Alternatively, fine-scale electrodes have been shown an effective method for increasing the thrust. For example, Abe et al. [6] found an increase in the momentum transfer (i.e., thrust) though the use of thinner copper tape electrodes. Similarly, Hoskinson et al. [7] demonstrated an exponential increase in measured thrust as the diameter of the wire electrode decreased from 0.40 mm to 0.11 mm. These increases may be explained by considering the electric field around a conducting wire: for a cylindrical conductor at a given potential, the electric field is inversely proportional to the wire's radius ($E \propto 1/r$).

Through miniaturization of the DBD actuator geometries (both electrode size and dielectric thickness) we aim to leverage an increase in electric field in an effort to improve the fluidic control authority and actuator effectiveness. In this paper we demonstrate the successful fabrication of microscale DBD devices and experimentally analyze their power consumption, velocity distribution, and thrust production with reduced-scale geometries. We then compare our device performance with reported data from macroscale DBD plasma actuators.

## EXPERIMENT

The devices are constructed using 10-mm-long thin-film titanium electrodes and a 10-μm-thick polyimide dielectric on glass substrates (500 μm thick) using previously reported microfabrication techniques [8]. The electrodes are created using sputter deposition, and the polyimide layer is spin-coated and heat-cured. The powered (top) electrodes are 1 μm thick and range from 10 μm to 500 μm in width. The ground (bottom) electrodes are 0.1

µm thick and range from 10 µm to 1 mm in width. All of the devices have a 100 µm lateral gap (offset) between the electrodes. The leads are extended such that the contact probes do not interfere with the field-of-view for velocity measurements. Three devices used in these experiments are shown in Fig. 2, showing the characteristic purple glow discharge under atmospheric conditions.

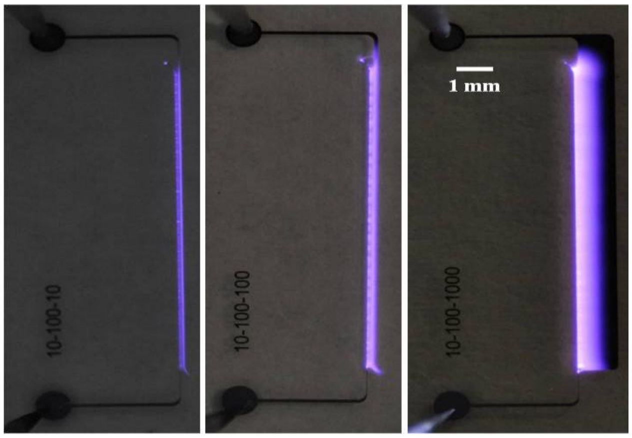


*Figure 2: Some devices used for the experimental data (shown during discharge). The nomenclature corresponds to the width of the powered electrode (left electrode), electrode gap, and grounded electrode (right electrode), respectively.*

For testing, a high-voltage sinusoidal input is generated using a function generator (Tektronix AFG3022B) and amplifier (Trek 30/20A). All of the tests are conducted at a frequency of 1 kHz. A high-voltage probe (Tektronix P6015A) measures the voltage amplitude and a current monitor (Pearson 2100) is used for current measurements. A digital oscilloscope (Tektronix DPO3014) captures both of these signals, and the average power dissipated is computed by integrating the voltage-current product over 200 periods.

Particle image velocimetry (PIV) is used to measure the instantaneous velocities induced by the plasma discharge. The PIV setup consists of a Nd:YAG laser (New Wave Research) and uses a high-speed camera (LaVision Imager Pro X 4M) with a 105 mm macro lens. The laser sheet is approximately 1 mm thick, and is positioned at the mid-point of the electrodes. The time interval (*dt*) between image pairs is adjusted for a maximum particle displacement of 5 - 7 pixels. Ondina oil is used for the PIV seed material, having a mean particle diameter of 0.8 µm (TSI 9302 atomizer). Data is processed using LaVision's DaVis 7.2 software (mean background subtraction, multi-pass cross-correlation, outlier rejection), and the velocity field is time-averaged using 80 image pairs. The resulting vector resolution is 78.6 µm (for both x and y directions) using a 20 mm wide field-of-view.

Pitot measurements are used to verify the PIV data, using a glass pipette probe with 1.5 mm outer diameter and 1.0 mm inner diameter. A differential pressure transducer (Furness Controls FCO332) with accuracy of 0.01 Pa is used to measure the stagnation pressure, which is converted to velocity using the formula, $p - p_{atm} = 0.5\rho v^2$, where the density of air $\rho$ = 1.18 kg/m$^3$ (at 25 °C), and $v$ is the fluid velocity (m/s). A traverse system allows precise control for incrementing the probe location. The absolute position relative to the substrate, however, is limited in accuracy by the initial manual alignment.

Direct force measurement of the time-average plasma-induced thrust is performed using a torsional balance similar to that of [9]. The balance measures the plasma actuator thrust as an angular deflection acting in opposition to torsion springs. The displacement is measured using a reflectance-based optical displacement sensor (PhilTec D100) having 40 nm resolution. Based on the measured displacement $x$, the angular deflection $\theta$ is calculated as $\theta = \arcsin(x/l)$ (radians), where $l$ is the moment arm length (m). From here, the force $F$ may be computed as $F = k_\theta \theta / l$ (N), where $k_\theta$ is the rotational spring constant (N·m/rad). A viscous oil bath is used to damp out extraneous vibrations to facilitate force measurements with an estimated resolution of 35 nN.

The balance is calibrated using an electrostatic force between parallel plate electrodes, which is presumed "known" via finite-element computation using Ansys Maxwell 2D. The rotational spring constant obtained through electrostatic calibration is validated via log decrement analysis of the transient response to a step input. Using the extracted natural frequency $\omega_n$ (rad/s) from the balance and the measured mass inertia $I$ (kg·m$^2$), the rotational spring constant may be computed as $k_\theta = \omega_n^2 I$ for comparison. The balance has a natural frequency of 0.37 Hz and a rotational spring constant of 0.292 N·m/rad.

## RESULTS

Figure 3 shows the power consumed for microscale DBD devices with varying electrode widths operated at 1 kHz. The power consumption shows little dependency on the exposed electrode width. However, slight differences are observed for the grounded electrode width; a wider ground electrode slightly increases the power dissipation. The ability to store charge (and thus dissipate power) is related to the area of the ground electrode. The data is fit with a power-law curve to examine the dependency of power on the applied voltage. The fit lines indicate the power scales exponentially with the voltage, with the exponent α ranging from 3.1 to 3.6 in these data. The average power consumed (per unit length of electrode) reaches 15 W/m at 5 kV$_{pp}$ and 1 kHz.

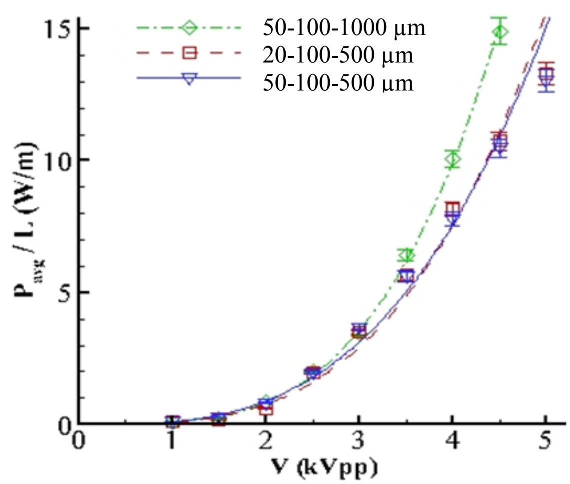


*Figure 3: Power consumed for DBD devices with varying electrode geometries plotted against applied voltage, operated at 1 kHz. The nomenclature corresponds to the width of the powered electrode, electrode gap, and grounded electrode, respectively.*

PIV data is shown in Fig. 4 for a microscale DBD actuator with a 10-µm-wide exposed electrode and 1-mm-wide ground electrode. The actuator geometry and electrode widths are also indicated at the bottom of the velocity contour plot for reference. The velocity magnitude reaches up to 2 m/s in the region near the electrodes, and a wall jet is established that extends over 15 mm downstream. The wall jet is similar in profile to those produced using macroscale DBD actuators.

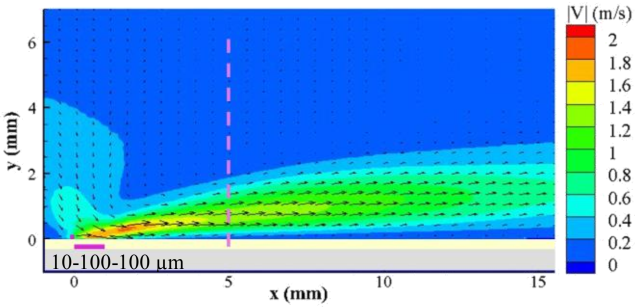


*Figure 4: PIV data for devices with a 10-μm-wide powered electrode and a 1-mm-wide grounded electrode. The electrode locations and geometry are indicated at the bottom of the figure; the vertical dashed line indicates the downstream location of the extracted velocity profile for comparison with pitot measurements.*

To validate the PIV results, pitot measurements were made 5 mm downstream from the edge of the powered electrode (location indicated with dashed vertical line in Fig. 4). Figure 5 compares the results from the velocity computed from pitot measurements with an extracted profile from PIV data. The pitot measurements show good agreement with the PIV data, with slight discrepancy between the vertical location of the data points. The offset between the PIV data and pitot measurement is most likely attributed to the 1 mm diameter of the pitot tube over which the pressure measurement is averaged. Error in the initial manual alignment of the pitot tube may also contribute to the data offset.

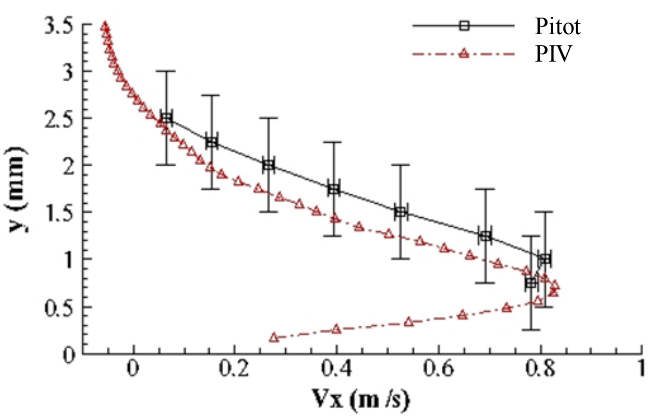


*Figure 5: Velocity profile from pitot measurements at x = 5 mm downstream compared with the extracted PIV velocity profile for a micro DBD actuator. Vertical error bars correspond to the 1 mm diameter of the pitot probe; horizontal error bars represent velocity measurement error.*

Measurements from the torsion balance force tests are shown in Fig. 6 for an actuator with a 10-μm-wide powered electrode and 100-μm-wide ground electrode. The plot shows the optically measured displacement as a function of time for various plasma excitations. Calibration measurements are made using built-in calibration electrodes for pre- and post-experiment comparison. The first two pulses correspond with a 50 V and 100 V potential applied across the calibration electrodes, providing electrostatic force and causing the balance to deflect toward the fixed electrode (away from the sensor). Following the calibration pulses, the actuator is successively stepped up in voltage from 4 to 6.5 kVpp in 0.5 kVpp increments. Each voltage is applied for approximately 10 seconds before turning off the actuator. Post actuator calibration is then performed for two purposes: (1) for comparison with the pre-calibration measurements for experimental consistency and (2) to provide increased resolution by using several voltages (30 – 70 V with 10 V increments) that produce displacements in the range of those measured using the actuator.

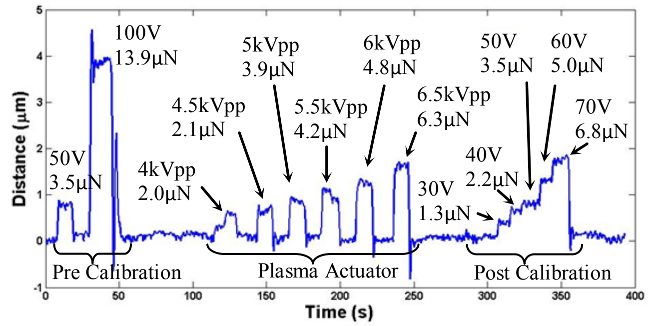


*Figure 6: Displacement measurements from torsional force balance for an actuator with a powered electrode width, gap and ground electrode width of 10, 100, and 100 μm, respectively. Electrostatic calibration is performed before and after each actuator tested using parallel plate electrodes.*

Using the measured deflections from the DBD actuator and comparing with the calibration measurements, the thrust is extracted for the different excitation voltages. Figure 7 plots the average force normalized by the electrode length against applied voltage for three actuators with different ground electrode widths. The device with the 1 mm wide ground electrode produced the greatest force, up to 3 mN/m (force normalized by electrode length). As observed in the power consumption data, devices with wider ground electrodes consumed slightly more power, which follows along with the increase in force observed here for the device with the largest ground electrode.

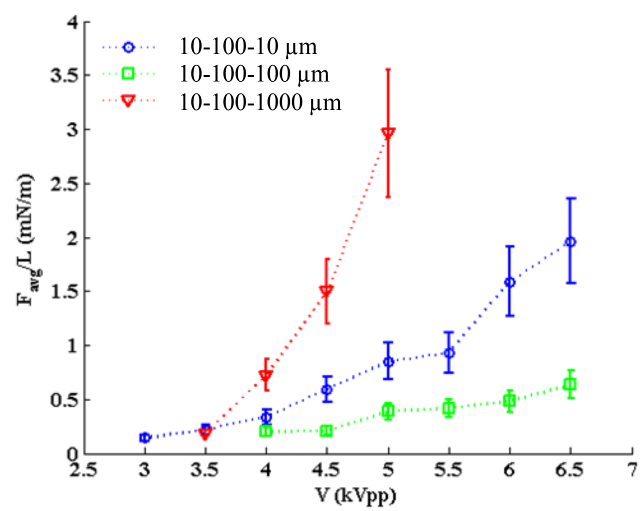


*Figure 7: Average force measured for three actuators having different ground electrode widths. The devices all have 10-μm-wide exposed electrodes and a 100-μm-wide gap. The force is normalized by the electrode length (l = 10 mm).*

The results from the microscale actuators are compared with reported macroscale DBD actuator performance [6] and summarized in Table 1. The actuator volume and mass are computed based on the DBD materials and geometries provided in [6], with electrode length normalized to 1 m. The first row reports the actuator thrust effectiveness; here, the macroscale actuator indicates similar thrust and power values to the microscale actuator, and both actuators demonstrate equivalent thrust effectiveness. The fourth row of data reports the velocity effectiveness; the microscale actuator provides an 86% increase compared with [6]. On a per-volume or per-mass basis, the micro actuator out-performs the macro actuator in both thrust and velocity metrics. This is attributed to the extreme size reduction of the microscale devices, in addition to the reduction in power consumption. The thick dielectric layer (few millimeters) generally utilized for macro DBD actuators governs the voltage, and in-turn, the power required to generate a wall jet. Employment of a thinner dielectric layer (10 μm) and miniaturized electrodes allows the micro actuator to produce velocities on the order of macroscale actuators with a significant reduction in size and mass.

*Table 1: Micro- and macro-DBD actuator performance metrics; comparing actuator thrust and velocity to power consumption, device geometry and material properties.*

| **Performance Metrics** | **Micro-DBD Vmax = 2 m/s Force = 3 mN/m Pavg = 15 W/m (5 kVpp, 1 kHz)** | **Macro-DBD [6] Vmax = 1.4 m/s Force = 3.9 mN/m Pavg = 20 W/m (20 kVpp, 1 kHz)** |
|---|---|---|
| Thrust “Effectiveness” [Force per Normalized Power] (mN/W) | 0.20 | 0.20 |
| Thurst Density [Force per Actuator Volume] ($mN/m^3$) | $5.29 \times 10^6$ | $6.84 \times 10^4$ |
| Thrust per Actuator Mass | 0.215 | $4.10 \times 10^{-3}$ |
| Velocity “Effectiveness” [Velocity per Normalized Power] (m/s) / (W/m) | 0.13 | 0.07 |
| Velocity per Actuator Volume (m/s) / $m^3$ | $3.53 \times 10^6$ | $2.46 \times 10^4$ |
| Velocity per Actuator Mass (m/s) / g | 1.41 | $1.44 \times 10^{-2}$ |

To further improve the actuator thrust effectiveness and thrust density (force per actuator volume), the dielectric gap should be reduced from 100 μm as reported here to few microns. The breakdown voltage for generating discharge is governed by the distance between the electrodes. Reducing the electrode gap and/or the dielectric layer thickness increases the field strength across the electrodes, leading to lower breakdown voltages and reducing the power required to operate DBD plasma actuators.

## CONCLUSION

In conclusion, we have demonstrated successful operation, flow inducement, and thrust generation of DBD devices having microscale dimensions. Devices that were operated at 5 $kV_{pp}$ and 1 kHz consumed 15 W/m on average. The power consumption scales with $V^{3.1\text{-}3.6}$ indicating that the microscale devices follow similar power trends to macroscale DBD actuators [4]. The reduction in power is attributed to the reduction in the necessary breakdown voltage for discharge gained from using a thin dielectric layer. The fluid velocities reached 2.0 m/s and the thrust was up to 3 mN/m. The actuator “effectiveness”—output per consumed power—was used to compare microscale and macroscale DBD actuators. The microscale actuators demonstrate equal thrust effectiveness to macroscale devices, indicating that the DBD actuator thrust performance scales linearly with size reduction. The velocity effectiveness of microscale actuators is 86 % greater than that of the macroscale DBD actuator.

Overall, the microscale DBD actuator induced velocity, thrust, and power consumption scale favorably with size reduction. The compact size, low mass, and lower voltage requirements of the microscale actuators make them implementable with minimal weight penalty. Furthermore, arrays of micro-DBD actuators could be constructed in flexible substrates (e.g. polyimide) for attachment on a curved surface, such as an airfoil.

## ACKNOWLEDGEMENTS

This work was supported in part by ARO Grant W911NF-09-1-0511 and AFOSR Grant FA9550-09-1-0416. Travel support has been generously provided in part by the Transducer Research Foundation. The authors also gratefully acknowledge the assistance from the staff of the UF Nanoscience Research Facility.

## REFERENCES

[1] F.O. Thomas, T.C. Corke, M. Iqbal, A. Kozlov, and D. Schatzman, “Optimization of Dielectric Barrier Discharge Plasma Actuators for Active Aerodynamic Flow Control”, AIAA J. 47, 9 (2009).
[2] E. Moreau, “Airflow Control by Non-thermal Plasma Actuators”, J. Phys. D: Appl. Phys. 40, 605 (2007).
[3] T.C. Corke, C.L. Enloe, and S.P. Wilkinson, “Dielectric Barrier Discharge Plasma Actuators for Flow Control”, Annu. Rev. Fl. Mech. 42, 505 (2010).
[4] C.L. Enloe, T.E. McLaughlin, R.D. VanDyken, K.D. Kachner, E.J. Jumper, and T.C. Corke, “Mechanisms and Responses of a Single Dielectric Barrier Plasma Actuator: Plasma Morphology”, AIAA J. 42, 3 (2004).
[5] M. Forte, J. Jolibois, J. Pons, E. Moreau, G. Touchard, and M. Cazalens, “Optimization of a Dielectric Barrier Discharge Actuator By Stationary and Non-stationary Measurements of the Induced Flow Velocity: Application to Airflow Control”, Exp. Fluids 43, 917 (2007).
[6] T. Abe, Y. Takizawa, S. Sato, and N. Kimura, “Experimental Study for Momentum Transfer in a Dielectric Barrier Discharge Plasma Actuator”, AIAA J. 46, 9 (2008).
[7] A.R. Hoskinson, N. Hershkowitz, and D.E. Ashpis, “Force Measurements of Single and Double Barrier DBD Plasma Actuators in Quiescent Air”, J. Phys. D: Appl. Phys. 41 (2008).
[8] J.C. Zito and D.P. Arnold, “Fabrication and Electrical Characterization of Microscale Dielectric Barrier Discharge Devices”, Tech. Dig. Solid-State Sensors, Actuators, and Microsystems Workshop, Hilton Head Isl., SC, 6/4-7/2010.
[9] M. Gamero-Castano, “A Torsional Balance for the Characterization of MicroNewton Thrusters”, Rev. Sci. Inst. 74, 10 (2003).

## CONTACT

*J.C. Zito, tel: +1-352-392-1484; jcz@ufl.edu